Int J Adv Struct Eng (2015) 7:341–352
DOI 10.1007/s40091-015-0102-9

ORIGINAL RESEARCH

RC beams shear-strengthened with fabric-reinforced-cementitious-matrix (FRCM) composite

Giovanni Loreto[1] · Saman Babaeidarabad[2] · Lorenzo Leardini[3] · Antonio Nanni[4]

Received: 7 December 2014 / Accepted: 20 July 2015 / Published online: 7 August 2015

Abstract The interest in retrofit/rehabilitation of existing concrete structures has increased due to degradation and/or introduction of more stringent design requirements. Among the externally-bonded strengthening systems fiber-reinforced polymers is the most widely known technology. Despite its effectiveness as a material system, the presence of an organic binder has some drawbacks that could be addressed by using in its place a cementitious binder as in fabric-reinforced cementitious matrix (FRCM) systems. The purpose of this paper is to evaluate the behavior of reinforced concrete (RC) beams strengthened in shear with U-wraps made of FRCM. An extensive experimental program was undertaken in order to understand and characterize this composite when used as a strengthening system. The laboratory results demonstrate the technical viability of FRCM for shear strengthening of RC beams. Based on the experimental and analytical results, FRCM increases shear strength but not proportionally to the number of fabric plies installed. On the other hand, FRCM failure modes are related with a high consistency to the amount of external reinforcement applied. Design considerations based on the algorithms proposed by ACI guidelines are also provided.

Keywords FRCM · Reinforced concrete · Repair · Shear · Strengthening

List of symbols

A_f	Area of fabric reinforcement by unit width (mm^2/mm)
E_f	Tensile modulus of elasticity of the cracked FRCM specimen (GPa)
V_c	Contribution of the concrete to the nominal shear strength (N)
V_f	Contribution of FRCM to the nominal shear strength (N)
V_n	Nominal shear strength (N)
V_s	Contribution of steel reinforcement to nominal shear strength (N)
b	Web width (mm)
d	Distance from extreme compression fiber to centroid of tension reinforcement (mm)
d_f	Effective depth of the FRCM shear reinforcement (mm)
f_{fu}	Ultimate tensile strength of FRCM (MPa)
f_{fv}	Design tensile strength of FRCM shear reinforcement (MPa)
s	Center-to-center spacing of shear reinforcement (mm)
ε_{fv}	Design tensile strain of FRCM shear reinforcement (mm/mm)
ε_{fu}	Ultimate tensile strain of the FRCM (mm/mm)

Introduction

During the last decades opportunities for retrofit/rehabilitation of existing structures have constantly increased in the world of civil engineering due to the need of ensuring

✉ Giovanni Loreto
giovanni.loreto.gl@gmail.com;
giovanni.loreto@ce.gatech.edu

[1] Department of Civil and Environmental Engineering, Georgia Institute of Technology, 790 Atlantic Drive, Room 5139d, Atlanta, GL 30332, USA

[2] Department of Civil Engineering, Science and Research Branch, Islamic Azad University, Tehran, Iran

[3] Department of Architecture, Building Environment and Construction Engineering, Politecnico di Milano, Piazza Leonardo da Vinci 32, 20133 Milan, Italy

[4] Department of Civil, Architectural, and Environmental Engineering, University of Miami, 1251 Memorial Drive, Room MEB 325, Coral Gables, FL 33146, USA

long-lasting performance of constructed facilities and/or meeting the demands of more stringent design standards. In particular, the collapse of reinforced concrete (RC) members due to shear deficiency is catastrophic and occurs suddenly with no advance warning of distress. Existing RC beams have often been found to be deficient in shear and in need of strengthening. Different materials and construction techniques are available for retrofit/rehabilitation and among them the most widely known involves the use of externally-bonded fiber-reinforced polymer (FRP) composites, which are formed by a polymer matrix reinforced with continuous and unidirectional fibers. Despite its effectiveness as a strengthening system (Fib Bulletin 2001), the presence of an epoxy binder in FRP has some drawbacks: lack of vapor permeability, poor behavior at service temperatures above the glass transition temperature, incompatibility with the substrate when wet, sensitivity to low temperature installation, and difficult reversibility (Triantafillou and Papanicolaou 2006; Papanicolaou et al. 2008; Aldea et al. 2007). In order to overcome these limitations, a new class of composites has emerged under the name of fabric-reinforced-cementitious-matrix (FRCM) materials by substituting the organic resin of the FRP system with a cementitious-based binder. FRCM is made by a sequence of two or more layers of cement-based matrix reinforced with single or multiple open fabrics made of dry fiber strands. FRCM has been reported in the technical literature using different acronyms (Ombres 2011) and often compared to FRP strengthening (Papanicolaou et al. 2008). By changing the nature of the matrix, differences between FRP and FRCM systems were found with respect of the level of impregnation of the fibers and mechanisms of failure. In the FRP systems, the organic binder ensures a full impregnation (wetting) of the fibers, whereas in FRCM, the cement-based binder is not able to penetrate through the fiber strands. Based on this peculiarity, D'Ambrisi and Focacci (2011) observed three possible failure modes when the FRCM was applied as a strengthening system: slippage of the fabric within the matrix, delamination of the FRCM from the substrate, and fracture surface within the concrete.

Evidence of the FRCM potential when used as a strengthening system is provided by Nanni (2012) through a description of field applications in different parts of the world. Moreover, recent experimental and theoretical works have shown the effectiveness of FRCM for confinement of RC elements and, shear and flexural strengthening of RC beams, slabs and masonry elements subjected to in-plane and out-of-plane load (Babaeidarabad et al. 2014; Loreto et al. 2013; Triantafillou and Papanicolaou 2006; Parisi et al. 2013).

Criteria for evaluation and characterization of the FRCM were issued by the International Code Council Evaluation Service (ICC-ES) in a document titled "Acceptance Criteria for Masonry and Concrete Strengthening Using Fiber-Reinforced Cementitious Matrix (FRCM) Composite Systems" (AC434 2013). This document addresses FRCM properties such as: tensile, flexural, and shear capacities; performance of FRCM under environmental exposures; performance under exposure to fire; and, structural design procedures. Following the test protocols established by AC434 (2013), the tensile characteristics to be used for analysis and design of FRCM strengthened RC members were derived for this project.

Similarly, American Concrete Institute (ACI) Committee 549—"Thin Reinforced Cementitious Products and Ferrocement" has completed a new design and construction guide that was published in late 2013 (ACI 549.4R-13 2013). This document was used for the interpretation of the experimental results.

Based on the increased interest in FRCM, an extensive experimental program was undertaken in order to understand and characterize this composite when used as a strengthening system. In this paper, results on the behavior of the FRCM used for shear strengthening of RC beams are presented. The experimental results were used to validate the analysis and design algorithms available in ACI549.4R-13 (2013).

Background

The mechanical properties of FRCM materials have been addressed in a series of publications by various researchers. Detailed analysis of the tensile mechanical response of these composites reveals that micro-cracking and crack distribution are two main internal features that result in toughening mechanisms (Peled and Mobasher 2007).

The stress–strain experimental behavior can be idealized with a bilinear curve (Fig. 1) in the case a clevis-type gripping system is used as per AC434 (2013). The first branch, which reflects the initial response of an un-cracked

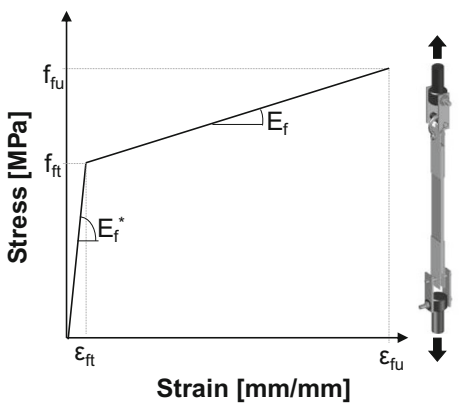

Fig. 1 Stress–strain curve for FRCM in tension

coupon, represents the elastic tension behavior of the mortar. The second one corresponds to the FRCM cracked behavior until failure by slip of the fabric (Arboleda et al. 2012; Loreto et al. 2013).

When used as a flexural strengthening system, FRCM behaves like an external tensile reinforcement for RC elements. When a flexural crack occurs inside the concrete due to its low tensile capacity, the tensile stresses released by the concrete are transferred to the strengthening material by interfacial bond. As the applied load increases together with the tensile stress in FRCM, the bond between the fabric and its matrix becomes critical. When the shear stress applied on the FRCM reaches its maximum capacity, the strengthening system fails (Ombres 2012). Moreover, it was observed that specimens with low level of strengthening fail due to fabric slippage, whereas specimens with higher level of strengthening fail due delamination between FRCM and the concrete substrate. Both the slippage and delamination failure modes make it impossible to attain fiber rupture (Ombres 2011; Loreto et al. 2013).

Brückner et al. (2006) demonstrated how thin layers of concrete with fabric reinforcement can be used for strengthening of RC members improving serviceability and shear capacity with reduction of deflection and crack width. Problems related to the force transfer mechanisms between the external strengthening system and the concrete substrate were also investigated. Tests were performed to describe the relationship between shear loading and deformation, as well as the necessary bond length and the transferable bond forces. Investigations proved that relatively short bond lengths were sufficient for the anchorage of the strengthening.

Triantafillou and Papanicolaou (2006) experimentally and analytically investigated the use of FRCM to increase the shear resistance of RC members under monotonic or cyclic loading. They concluded that FRCM jacketing provides substantial gain in shear resistance. This gain was higher as the number of layers increased and sufficient to transform shear-type failure to flexural-type failure.

Al-Salloum et al. (2012) investigated the use of basalt-FRCM as a means of increasing the shear resistance of RC beams. The studied parameters included: two different mortar types (cementitious and polymer-modified cementitious mortars), the number of reinforcement plies and their orientation. It was concluded that FRCM provides substantial gain in shear resistance. This gain was directly dependent upon the number of fabric plies installed.

Experimental study

The objectives of the experimental program were to: (a) provide a better understanding of the effectiveness of shear reinforcement offered by the addition of FRCM; (b) analyze the failure modes experienced by FRCM strengthened elements; and, (c) investigate the FRCM load transfer mechanism.

The experimental program was carried out by casting, strengthening and testing under three-point bending, 18 beams heavily reinforced in flexure to ensure shear deficiency.

The parameters considered were: two concrete compressive strengths (i.e., L = low = 28 MPa; H = high = 40 MPA) and the number of fabric plies (i.e., zero, one and four). Table 1 shows the test matrix where three identical repetitions were performed for each different configuration. Specimens were identified using the "A_B_C" format where: "A" denotes the concrete strength (L for low and H for high); "B" denotes the number of fabric plies (0, 1 or 4); and "C" denotes the replicate number (1–3 or average).

Table 1 Shear beams test matrix

Specimen ID	Type of concrete	FRCM plies
L_0_X	L	0
L_1_X	L	1
L_4_X	L	4
H_0_X	H	1
H_1_X	H	1
H_4_X	H	4

X three repetitions, L low-strength, H high-strength

Test specimen and materials

Specimens were constructed and tested in the Structures and Materials Laboratory at the University of Miami. Details of the reinforcement are shown in Fig. 2. All specimens were 1829 mm long with a rectangular cross-section 306 mm deep and 152 mm wide. Micro-composite multi-structural formable steel (MMFX) was used as longitudinal tensile reinforcement which consisted of four 19.1 mm diameter bars placed in two rows with nominal area of 286 mm^2, nominal yield strength of 690 MPa and modulus of elasticity of 200 GPa. Stirrups were mild steel with nominal yield strength of 276 MPa, modulus of elasticity of 200 GPa, diameter of 5.7 mm with nominal area of 26 mm^2 and spacing of 125 mm. At the top side of the beam, two 9.5 mm diameter bars of the same mild steel were used to also facilitate the moving and the installation of the steel cages during casting.

Beams were cast in disposable plywood molds. The bottom corners were rounded with a radius of 20 mm using wood molding strips in order to avoid grinding before FRCM installation. The beams were made from two concrete batches. The average concrete compressive strength was determined in accordance with ASTM C39 (2012) by testing nine cylinders with a nominal diameter of

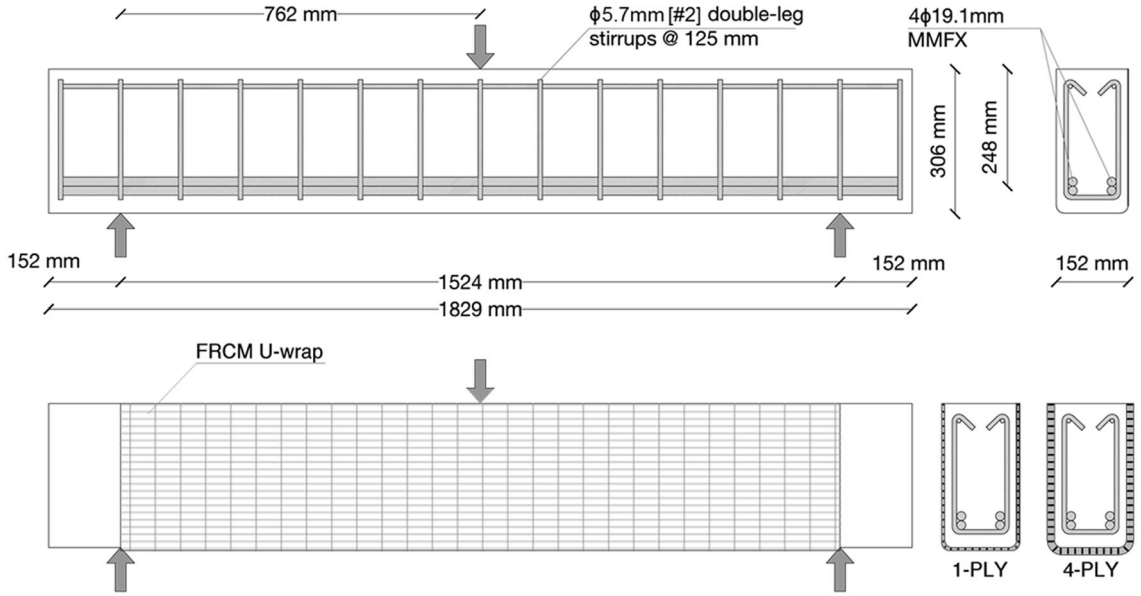

Fig. 2 Beam specimen layout

101.6 mm for each type of concrete. The average strength of the two batches was 29.13 and 42.91 MPa, respectively, with associated standard deviations of 1.01 and 1.84 MPa. Concrete moduli of elasticity were 29.5 and 30.4 GPa for low and high strength concrete, respectively. Specimens were cured under the same conditions for 6 days before the mold was stripped and then left for 28 days in the laboratory environment.

Before bonding FRCM to the concrete surface, dust and loose particles were removed by compressed-air cleaning. The concrete surface was wetted to a saturated surface dry (SSD) condition. FRCM was then installed in accordance with the manufacturer's instructions.

FRCM consisted of a matrix (Fig. 3a) made of portland cement and a dosage of dry polymers lower than 5 % in weight and reinforced with dry-fiber fabrics (Fig. 3b). The binder to water ratio was 3:1 by weight, resulting in plastic consistency and good workability. Polyparaphenylene benzobisoxazole (PBO) fibers were used for the primary direction (PD) and secondary direction (SD) strands of the fabric. The PBO fabric was made of 10 mm and 20 mm spaced strands with nominal areas by unit with of 47.52 and 12.95 mm^2/m in the warp and weft directions, respectively. The free space between strands was 5 and 15 mm, and the nominal thickness in the two strand directions was 0.046 and 0.011 mm, respectively. Figure 3b, c show details and architecture of the fabric.

According to Annex A of AC434 (2013) tensile coupons of 410 × 51 × 10 mm were tested to characterize the tensile behavior of the composite system. The following parameters based on net fabric area were obtained as representative of the tensile behavior of the FRCM system:

- tensile modulus of elasticity of the cracked specimen, E_f,
- ultimate tensile strain, ε_{fu},
- ultimate tensile strength, f_{fu}.

The mean, standard deviation and COV of the characteristic parameters were calculated based on five identical tests and summarized in Table 2. These FRCM parameters were used for the analysis and modeling of the strengthened RC elements.

Application of the mortar matrix was made in approximately 1.5–2 mm thick layers. After application of the first mortar layer on the concrete surface, the PBO fabric was applied and pressed into the mortar, which protruded through the perforations between strands. A second layer of mortar was then applied. The procedure was repeated three additional times in the case of four-ply FRCM. Beams were strengthened using a FRCM continuous U-wrap with the primary direction of the fabric oriented parallel to beam length (Fig. 2). Reasons for the choice of the configuration were: (a) ease of installation, (b) continuity of the fabric and no need for splices given the size of the roll, (c) contribution of PD and SD strands to the 45° crack opening, (d) additional flexure enhancement (even if not required here).

Test setup, instrumentation and test protocol

The three-point-bending test was performed with a clear shear span, a, of 762 mm (namely: distance from the loading point to the center of the support) and with a nominal shear span-to-depth ratio, a/d, of 3.0 for all the beams.

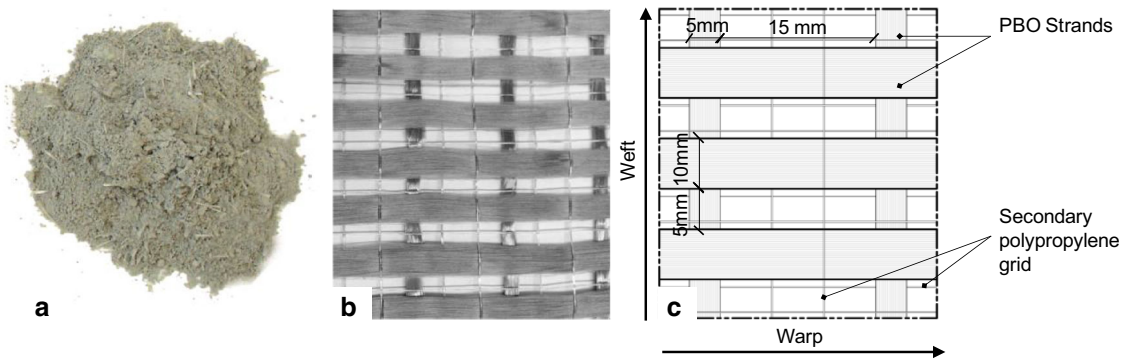

Fig. 3 Matrix detail (**a**), PBO fabric detail (**b**) and architecture (**c**)

Table 2 Results for PBO-FRCM tensile coupons tested according to AC434

FRCM property	Symbol	Units	Mean	Standard deviation	COV (%)
Modulus of elasticity of the cracked specimen	E_f	GPa	127	15	12
Ultimate tensile strength	f_{fu}	MPa	1664	77	5
Ultimate tensile strain	ε_{fu}	mm/mm	0.0176	0.0013	8
Analytical tensile strain $\varepsilon_{fv} \leq 0.004$	ε_{fv}	mm/mm	0.004	N/A	N/A
Analytical stress $f_{fv} = E_f \varepsilon_{fv}$	f_{fv}	MPa	510	N/A	N/A

Testing was performed using a mechanical screw-driven actuator with a maximum capacity of 1300 kN. Applied load was recorded using both the internal force transducer in the actuator and a load cell placed at one of the supports. Four linear variable differential transducers (LVDTs) were used to record deflections at the two supports and at mid-span allowing for the computation of net deflection at mid-span. Strain measurements were recorded using four strain gauges bonded in pairs to internal steel bars and concrete surface in compression. Two additional strain gauges were located on the FRCM lateral surface at the intersection between the 45° line from the point of application of the load and the mid-height of the cross section. Experimental data were gathered using a National Instruments data acquisition system running LabVIEW software.

All beams were tested monotonically. Load was applied in displacement control at a rate of 0.75 mm/min in a quasi-static loading and unloading pattern for a total of six complete cycles plus loading to failure. Load–deflection curves, initial cracking load, ultimate load, and deflection at initial concrete cracking and at steel yielding load were recorded.

Test results and discussion

A summary of test results for all beams are displayed in Table 3 (experimental and analytical shear capacities) and Table 4 (experimental strains and deflections). Each row with experimental values represents the average of the three repetitions and the corresponding standard deviation. Irrespective of the concrete strength, beams with the same level of reinforcement (control, one- and four-ply FRCM) performed similarly.

The control beams failed in compression shear, as expected, through the formation of diagonal cracks in the shear spans followed by crushing of the concrete in the compression zone next to the load application point. The average ultimate loads were 166.85 and 183.26 kN with relative standard deviations of 0.49 and 5.66 kN for low and high strength concrete, respectively. During control beam tests, no sudden drop in the load was recorded after diagonal cracking. This is attributed to the considerable contribution to shear resistance provided by both the stirrups crossing the crack and the strong dowel action provided by the MMFX longitudinal bars.

As expected the strengthened beams achieved a higher level of load. The average ultimate loads were equal to 203 and 231 kN with relative standard deviations of 3.78 and 12.05, and 251 and 295 kN with relative standard deviations of 8.66 and 7.09 kN, in the case of one-ply and four-ply FRCM, for low and high strength concrete, respectively. Strength enhancement, defined as the ratio between the maximum capacity of the strengthened beams and the control one, was found to be 121 and 151 % for beams with low-strength concrete and 126 and 161 % for beams with high-strength concrete with one-ply and four-ply FRCM, respectively.

Table 3 Average experimental and analytical shear capacities

Beam ID	Experimental			Analytical				
	Ave $P_{u,avg}$ kN	Std. dev. – kN	Enhancement $P_{u,avg,strengthed}/P_{u,avg,control}$ –	Theoretical $P_{u,th}$ kN	Enhancement $P_{u,th,strengthed}/P_{u,th,control}$ –	Exp./th. ratio $P_{u,avg}/P_{u,th}$ –	ACI 549 $P_{u,ACI549}$ kN	Enhancement $P_{u,ACI549,strengthed}/P_{u,ACI549,control}$ –
L_0_Ave	166.85	0.49	1.00	122.64	1.00	1.36	122.64	1.00
L_1_Ave	203.13	3.78	1.21	144.20	1.18	1.41	136.87	1.12
L_4_Ave	251.15	8.66	1.51	213.76	1.74	1.17	179.56	1.46
H_0_Ave	183.26	5.66	1.00	135.80	1.00	1.35	135.80	1.00
H_1_Ave	231.17	12.05	1.26	158.99	1.34	1.45	150.04	1.10
H_4_Ave	295.69	7.09	1.61	228.56	1.68	1.29	192.73	1.42

Table 4 Average strains and deflections

Beam ID	Micro-strain								Deflection @ max–load	
	$\mu\varepsilon_c$	Std. dev.	$\mu\varepsilon_s$	Std. dev.	$\mu\varepsilon_{FRCM\_h}$	Std. dev.	$\mu\varepsilon_{FRCM\_v}$	Std. dev.	Δ (mm)	Std. dev.
L_0_Ave	2150	366	1880	474	1240	N/A	5810	N/A	6.09	1.06
L_1_Ave	2630	891	1890	200	1580	N/A	5820	358	8.91	1.12
L_4_Ave	1870	175	2640	161	690	N/A	5370	715	8.95	1.26
H_0_Ave	2620	671	1690	167	N/A	N/A	N/A	N/A	6.28	0.53
H_1_Ave	2780	269	2220	170	720	N/A	6440	2140	7.50	0.50
H_4_Ave	2110	163	2820	212	910	156	6770	1300	7.59	0.09

N/A for strain = gages nonfunctioning; N/A for st. dev. = no value or only one value of strain available

Load–deflection

Figure 4 shows the three load–deflection envelopes generated for the control, one-ply and four-ply FRCM beams cast with high-strength concrete (low-strength concrete beams performed similarly). In these beams, the average values of deflection at maximum load were found to be equal to 6.3, 7.5 and 7.6 mm for control, one-ply and four-ply strengthened specimens, respectively (being 0.43, 0.41 and 0.08 mm the respective standard deviations). The stiffness (i.e., the slope of the load–deflection diagram) in the very first loading stage is similar for the control and one-ply FRCM specimen configurations, since the contribution of the FRCM to the moment of inertia of the uncracked cross-section can be considered negligible. Conversely, four-ply FRCM specimens were affected by the relatively larger amount of FRCM that contributed to increase the stiffness of the elements. The gain in strength was a function of the presence of the FRCM (also deflection at maximum load for strengthened beams is higher than in the control ones). Ultimate deflections decreased with the increasing of the concrete strength in strengthened specimens (Table 4).

Crack pattern and failure modes

Irrespective of the type of concrete, beams developed shear cracks according to three distinct patterns depending on the number fabric plies. Figure 5 shows the three recorded patterns along with the angles formed by the cracks for control, one-ply and four-ply specimens. In the case of four-ply FRCM, after completing the test, the U-wrap was peeled off to expose the crack pattern.

On control beams (Fig. 5a), shear cracks started to appear at a load approximately 60 % of the peak. As the load increased, two major shear cracks were observed widening and propagating towards the loading point till failure. The compression zone of the control beams was increasingly constricted by the cracks with a pattern typical of compression shear failure. A slight contribution of the arch effect was also evidenced with a direction of the shear cracks lower than 45° angle.

Increase in shear capacity was detected in every strengthened beam. In the case of one-ply FRCM, the crack pattern was similar to that of the control specimen (Fig. 5b) with cracks reflecting into FRCM and visible fiber strands slip (Fig. 6a, b).

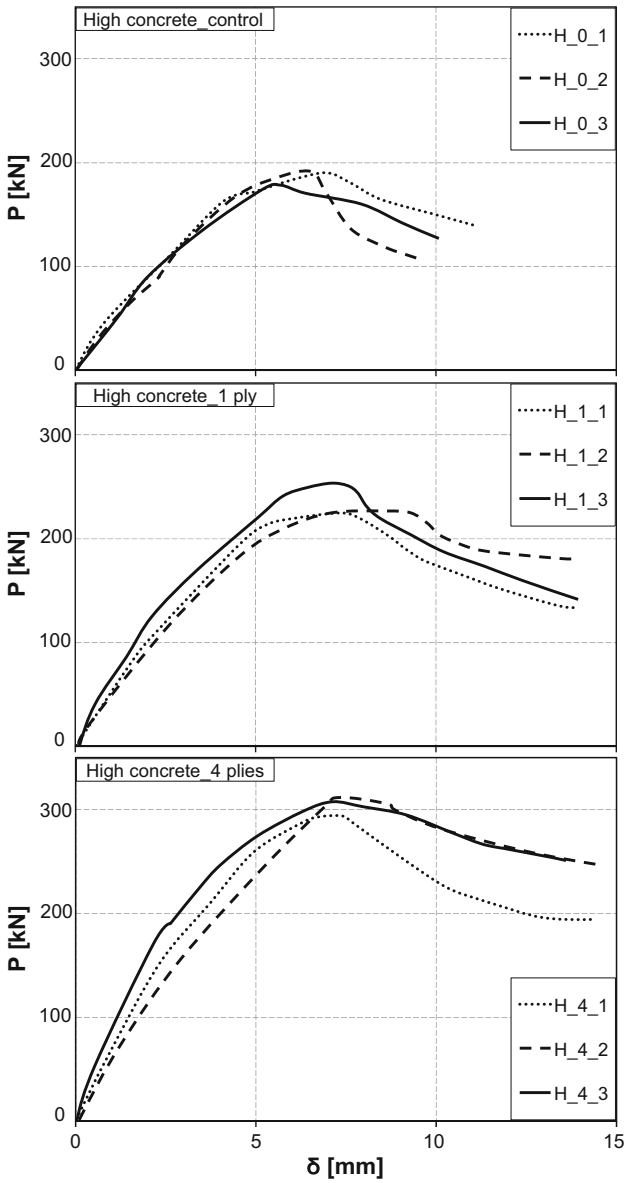

Fig. 4 Load–deflection diagrams for all high-strength concrete shear beams

On the specimens strengthened with four-ply FRCM, no visible shear crack was detected on the lateral side before collapse. However, during loading a cracking sound occasionally emitted from the beams. The sound increased in intensity as the beams were loaded closer to the maximum load. After completing the test, the FRCM was removed showing finer shear cracks that did not reflect on the FRCM exposed surface (Fig. 5c). The failure was revealed by a final shear crack inclined at an angle of about 45° towards the point of load application.

The failure mode was due to the partial delamination of the FRCM from the substrate. Bulging initiated in proximity of the loading knife and occurred on both beam sides followed by crushing of concrete (Fig. 5c, d). Due to the continuous FRCM U-wrap configuration, the tensile forces in the strengthening layers were transferred to the compression zone similarly to the contribution of internal stirrups.

Overall, FRCM strengthening did not alter the failure mode of the beams that remained compression shear.

Figure 7 shows the envelopes of load–deflection diagrams for high-strength concrete beams in which each curve represents the average envelope of the three experimental curves. A clear increase in ductility is visible on the beams strengthened with FRCM. A similar trend was visible in low-strength concrete beams. Three additional lines shown in Fig. 7 represent the predictions generated according to the ACI 549.4R-13 algorithms that will be later discussed.

Strain

Table 4 displays the average strain measurements collected at maximum load in compression (ε_c), tension (ε_s) and on lateral side mid-section (ε_{FRCM_h} and ε_{FRCM_v}). In all test configurations, the longitudinal steel never reached nominal yielding at failure.

In the case of the control specimens, the behavior of the strain gauges installed on the lateral surface was affected by the unpredictability of the crack-growing path, whereas, in the presence of FRCM, data collected from strengthened specimens showed less variability.

Strain readings from both the horizontal and vertical fiber strands indicate that the FRCM was not carrying high strain in the early stage of loading. However, a rapid strain gain was recorded in the final stage of loading following the formation of cracks.

Using the FRCM constitutive law, the values of strain gauges located on the FRCM lateral surface, ε_{FRCM_h} and ε_{FRCM_v}, were transformed into σ_h and σ_v, in order to describe the plane stress state at that point. In addition the shear stresses over a uniform rectangular cross section, τ_{xy}, subjected to a shear force (V) were computed as in Popov (1999):

$$\tau_{xy} = \frac{S \cdot Q(y)}{I \cdot b} \quad (1)$$

where τ_{xy} is the y-component of the shear stress on a surface perpendicular to the x-axis, y is the chord that represents the distance from the neutral axis of the fiber in which the shear stress is computed, b is the width of the cross-section at the level where the shear stress is determined, $Q(y)$ is the first moment of the area above y about the neutral axis, and I the moment of inertia. The latter needs to be calculated for every cross section and varies with the amount and size of cracks. However, a member critical in

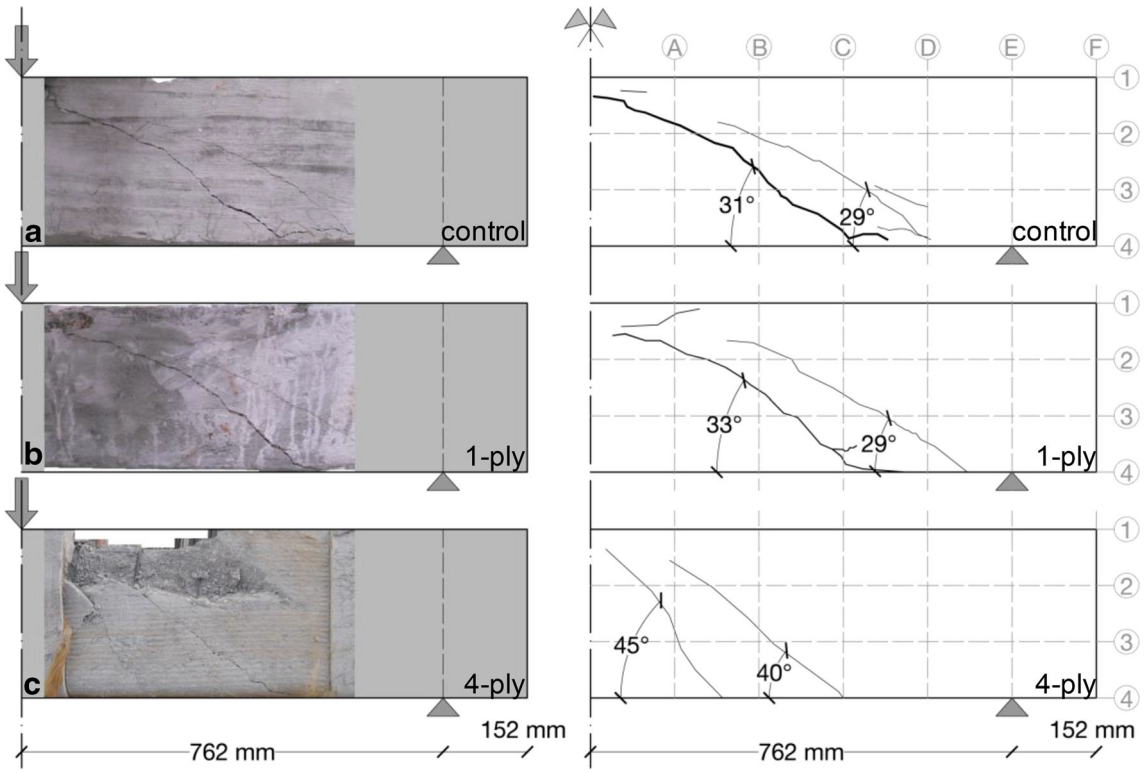

Fig. 5 Typical crack pattern for control, one-ply and four-ply FRCM beams

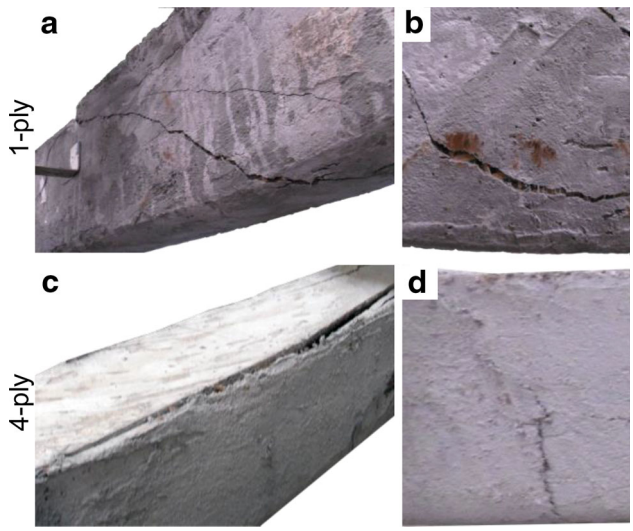

Fig. 6 Failure modes for one-ply and four-ply FRCM specimens

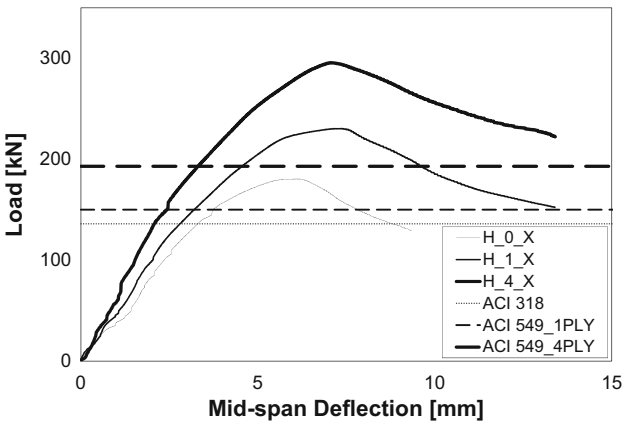

Fig. 7 Load–deflection envelope diagrams versus ACI549 predictions

shear has satisfactory bending capacity with an amount of flexural cracking relatively small in regions of high shear stresses. In these areas, cracks are generally limited or highly distributed (Carolin and Täljsten 2005). In addition, before the ultimate shear failure, the studied shear specimens did not show any large shear crack. In particular, in the case of specimens strengthened with four-ply FRCM, the crack pattern consisted of a cracked zone with many relatively small cracks spread over the studied area. When high degree of crack distribution prevails, the value of the moment of inertia in Eq. (1) is comparable to the value of moment of inertia calculated for a non-cracked cross section (Carolin and Täljsten 2005; Blanksvärd et al. 2009). Under these hypotheses, the shear stresses were computed as if parabolically distributed along the entire cross-section height where the maximum value, located at the mid-high of the cross section, is computed from Eq. (1). Specifically, $\tau_{max} = 3V/(2b{\cdot}d)$ being b and d the cross-section width and height, respectively.

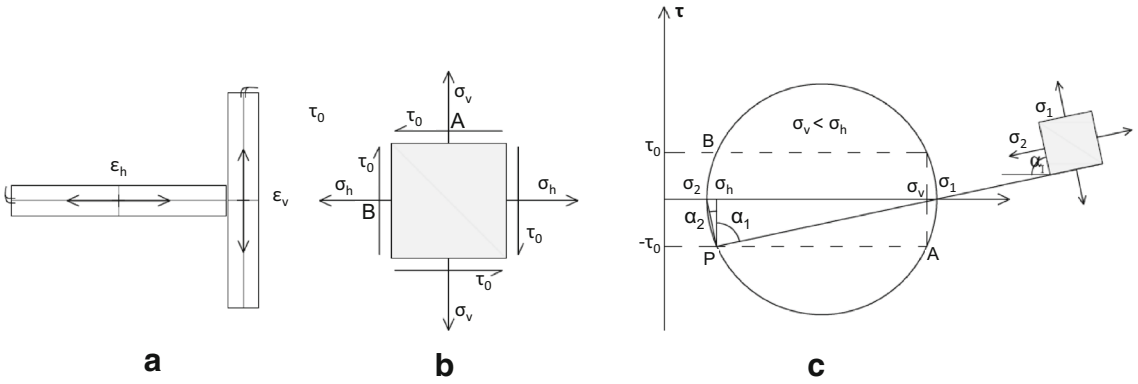

Fig. 8 Strain data acquisition (**a**), state of plain stress (**b**), and (**c**) principal stresses and Mohr's circle

Based on the geometrical properties of the Mohr's circle (Fig. 8a–c), the value of the principal stresses were calculated along with the principal tensile direction angle (α_I).

$$\alpha_I = \text{arctg}\left(\frac{\sigma_h - \sigma_{II}}{\tau}\right) \quad (2)$$

where σ_{II} represents the principal stress, τ the shear stress and σ_h the stress in the horizontal direction.

In Fig. 9a, the values of the vertical and horizontal strains, recorded on the lateral side mid-height, are plotted as a function of time along with the load throughout the entire duration of the test for beam H_1_1. In a second graph (Fig. 9b), the principal tensile direction angle and deflection values are plotted versus the applied load for the same beam.

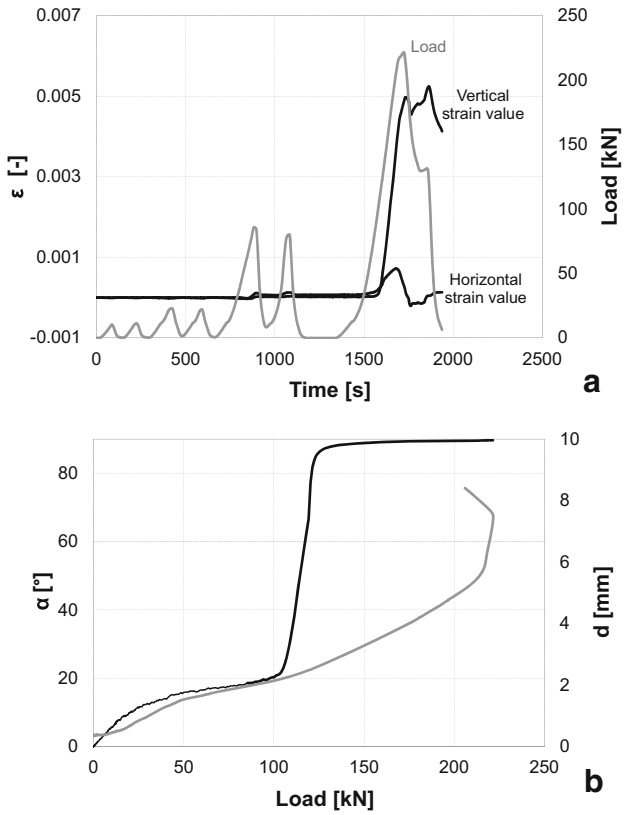

Fig. 9 Load and strain (ε_v and ε_h) versus time (**a**) and principal stress directions (α) and deflection (Δ) versus applied load (**b**) (H_1_1)

Looking at the first diagram, in the first six cycles the level of the vertical and horizontal strains on the FRCM were approximately zero. Consequently, the principal tensile direction angle was found to reach a maximum value of 20°. During the last load cycle, when the level of the load approached 60 % of the peak and the vertical direction strain became greater than the horizontal one, the principal tensile direction angle started to rotate clockwise. By increasing the load, the principal direction approaches the 90° angle (in other words perpendicular to the beam axis). This behavior indicates that for low level of load both the PD and SD of the FRCM strengthening system collaborate to increase of shear capacity, whereas, while approaching failure, the PD response becomes dominant. This behavior was consistently recorded throughout all tests.

Nominal capacity analysis

Analytical predictions of the beams are displayed in Table 3. The shear capacity was estimated superimposing the respective contributions of concrete (V_c), steel (V_s) and the external reinforcement (V_f). V_c and V_s expressions were based on ACI 318-11. Steel contribution was equal to 27.59 kN for all beams, whereas concrete contribution was found to be 33.73 and 40.31 kN for low and high concrete compressive strengths, respectively.

The FRCM shear contribution, V_f, was calculated in accordance to the ACI 549.4R-13, which provides design recommendations consistent with the provisions of AC434. The analysis considers FRCM as a shear reinforcement uniformly distributed along the depth, d, of the beam. As per ACI 549.4R-13, the ultimate tensile strain to be used for FRCM design considerations, ε_{fu}, is the average minus

one standard deviation of the values obtained from tensile tests conducted based on AC434 (2013) standard. In these tests the tensile stress–strain curve is initially linear until cracking of the cementitious matrix occurs, deviates from linearity and becomes linear again until failure by slippage (Loreto et al. 2013). Due to this mechanism that leads to failure before exhaustion of the fabric capacity, the plot can be idealized to a simple bilinear curve as reported in Fig. 1 from which the ultimate tensile strength and strain can be determined (AC434 2013, ACI 549.4R-13).

To calculate the shear contribution of FRCM, V_f, the average of the cracked modulus of elasticity, E_f, and the ultimate strain, ε_{fv}, were used according to Annex A of AC434 (2013). ε_{fv} and E_f, values were equal to 0.0163 mm/mm and 127,647 MPa, respectively.

According to ACI 549.4R-13, the ultimate strain cannot exceed 0.004, therefore this was the value used and the results reported in Table 3 in column $P_{u,ACI549}$. Furthermore, in order to verify the lever of accuracy of the analysis, the shear contribution of the FRCM was also estimated using the mean values of the material properties. The result of this analysis are also displayed in Table 3 under the column $P_{u,th}$.

The design tensile strength of the FRCM shear reinforcement, f_{fv}, was calculated in accordance with the simplified linear stress–strain trend as in Eq. (3):

$$f_{fv} = E_f \varepsilon_{fv} \tag{3}$$

The shear contribution of the FRCM reinforcement, V_f, is given by Eq. (4):

$$V_f = nA_f f_{fv} d_f \tag{4}$$

where n is the number of plies, d_f is the effective depth of the FRCM shear reinforcement and A_f is the area of fabric reinforcement by unit width effective in shear.

With regard to the area of fabric reinforcement, the PBO fibers used in this research were characterized by a PD and SD of the fiber strands with a ratio of approximately 4:1. ACI 549.4R-13 allows the combined contribution to shear strength of both fiber strands. Where both PD and SD are used to reinforce the same portion of a member, ACI 549.4R-13 imposes that at least the 50 % of the additional shear capacity due to the external reinforcement has to be provided by the fiber strands installed perpendicular to the member axis and, V_f has to be computed by superimposing the contributions of both parallel and perpendicular directions. The PBO fibers were installed with their primary direction oriented parallel to beam length and, therefore, the PD fibers could only carry 50 % of the total strengthening reinforcement. Based on this limitation, the effective-in-shear area of fibers (A_f) was considered in both directions equal to the SD amount. The analytical shear capacity was then evaluated based on the number of plies (one or four) installed.

In all cases the predictions underestimate the experimental strength of the FRCM-strengthened specimens. The ratios between the experimental, $P_{u,avg}$, and the analytical ultimate capacity, $P_{u,th}$ are reported in the last column of Table 3, whereas Fig. 7 provides a visual representation of the experimental values in comparison to $P_{u,ACI549}$. Both analysis yield rather conservative results in line with the performance of the one-ply FRCM tensile coupon, tested as per AC434 (2013), in which the failure was governed by the slip of the fiber strands within the cementitious matrix without rupture of the fibers.

Conclusions

The laboratory results demonstrate the technical viability of FRCM for shear strengthening of RC beams. Based on the experimental and analytical results, FRCM increases shear strength but not proportionally to the number of plies installed. The strength enhancement was found to be 121 and 151 % for beams with low-strength concrete and 126 and 161 % for beams with high-strength concrete with one-ply and four-ply FRCM, respectively. The performance improvement also included a gain in ductility.

FRCM failure modes were found to be related with a high consistency to the amount of external reinforcement applied. In particular slippage failure mode occurred for one-ply strengthened specimens while delamination from the substrate characterized the ones with four plies.

An analysis was performed in order to verify the level of accuracy of the ultimate shear capacity prediction according to the ACI 549.4R-13 (2013) guide. It is shown that prediction underestimates the enhancement due to FRCM strengthening because the tensile properties used in the analysis do not depend on fiber rupture but are based on the performance of the FRCM tensile coupon after the crack saturation zone.

Acknowledgments The authors gratefully acknowledge NSF for the support provided to the Industry/University Center for Integration of Composites into Infrastructure (CICI) under Grant IIP-0933537 and its industrial member Ruredil S.p.A., San Donato Milanese, Italy. Any opinions, findings, and conclusions or recommendations expressed in this material are those of the authors and do not necessarily reflect the views of the NSF.

Appendix: Design of RC concrete beam strengthened with four-ply FRCM

Calculate the analytical and design shear capacity of a RC concrete beam strengthened with four-ply FRCM according to ACI 549.4R-13 using actual geometry and material properties obtained from FRCM coupons and concrete cylinder. The shear capacity of a strengthened RC beam is the sum of the concrete, steel stirrup, and FRCM shear contribution.

Beam properties

Cross-section height	$h = 305$ mm
Cross-section effective height	$d = 248$ mm
Effective depth of shear reinforcement	$d_{fv} = 305$ mm
Web width	$b_w = 152$ mm
Compressive strength of concrete	$f'_c = 41.4$ MPa
Area of stirrup reinforcement	$A_{stirrup} = 25.7$ mm^2
Area of shear reinforcement	$A_v = 2A_{stirrup} = 51.4$ mm^2
Steel tensile yield strength	$f_y = 275.8$ MPa

FRCM properties

Area of fabric per unit width	$A_{f\_SD} = 0.011$ mm
Area of fabric per unit width	$A_{f\_PD} = 0.046$ mm
Design tensile strain (mean minus one standard deviation)	$\varepsilon_{fd} = 0.0163$ mm/mm
Tensile modulus of elasticity	$E_f = 128$ GPa
Design tensile strain of FRCM shear reinforcement	$\varepsilon_{fv} = \min(\varepsilon_{fd}, 0.044)$ mm/mm
Number of plies	$N = 4$

Concrete and steel stirrups contribution

$$V_c = 2\lambda\sqrt{f'_c}b_w d = 40.3\,\text{kN}$$

$$V_s = A_v f_{yt}\frac{d}{s_s} = 27.6\,\text{kN}$$

$$V_c + V_s = 67.9\,\text{kN}$$

Step 1: Calculate the FRCM system design material properties as per ACI 549.4R-13:

- Calculated design tensile strain: $\varepsilon_{fv} = 0.004$ mm/mm
- Calculated design tensile strength: $f_{fv} = E_f \times \varepsilon_{fv} = 510.6$ MPa

Step 2: Select the number of plies, *n, of the FRCM material to apply*

- Calculated total area of reinforcement: $A_{fTot\_PD} = 2A_{f\_PD} = 0.02$ mm $A_{fTot\_SD} = 2A_{f\_SD} = 0.09$ mm

Step 3: Calculate the contribution of the FRCM reinforcement to the shear strength:

$$V_f = n(A_{fTot_{SD}} + \min(A_{fTot_{SD}}, A_{fTot_{PD}}))f_{fv}d_{fv} = 28.5\,\text{kN}$$

Step 4: Calculate the total shear strength

- Calculate the shear strength of control RC beams: $V_{n,\text{Control}} = V_c + V_s = 67.9$ kN
- Calculate the shear strength of strengthened RC beams: $V_{n,\text{4-ply strengthened beams}} = V_c + V_s + V_f = 96.4$ kN

Step 5: Check maximum shear force

According to ACI 549.4R-13, the total shear strength provided by FRCM and steel reinforcement should be limited to the following:

$$V_s + V_f \le 8\lambda\sqrt{f'_c}b_w d = 56.1\,\text{kN} \le 161.2\,\text{kN}$$

Design provisions

According to ACI 549.4R-13 and ACI 562-13, the increment in shear strength is limited to 50 % of un-strengthened RC beam to limit the total force per unit width transferred to the concrete:

$$V_n = min(V_{n,4-\text{plystrengthenedbeams}}, 1.5V_{n,\text{Control}}) = 96.4\text{kN}$$

Additionally; the strength reduction factor ϕ_v should be equal to 0.75 as per ACI 318 and ACI 562:

- Design shear is computed according to the following: $V_{n,\text{Des.}} = \phi_v V_n = 72.3\,\text{kN}$

References

AC434:2013 – ICC-Evaluation Service (2013) Acceptance criteria for masonry and concrete strengthening using fiber-reinforced cementitious matrix (FRCM) composite systems. Whittier, CA

ACI Committee 549:2013 – American Concrete Institute (2013) Guide to design and construction of externally bonded FRCM systems for repair and strengthening concrete and masonry structures. 549.4R-13, Farmington Hills, MI

Aldea CM, Mobasher B, Jain N (2007) Cement based matrix–fabric system for masonry rehabilitation. ACI SP-244. In: Aldea CM (ed), pp 141–156

Al-Salloum Y, Elsanadedy H, Alsayed S, Iqbal R (2012) Experimental and numerical study for the shear strengthening of reinforced concrete beams using textile-reinforced mortar. J Compos Constr 16(1):74–90

Arboleda D, Loreto G, De Luca A, Nanni A (2012) Material characterization of fiber reinforced cementitious matrix (FRCM)

composite laminates. In: Proceedings of 10th international symposium on ferrocement and thin reinforced cement composite, Havana, Cuba, October 12–17, pp 113–120

ASTM C39/C39M (2012) Standard test method for compressive strength of cylindrical concrete specimens. ASTM International, West Conshohocken

Babaeidarabad S, Loreto G, Nanni A (2014) Flexural strengthening of RC beams with externally-bonded fabric-reinforced-cementitious-matrix (FRCM). J. Compos 18(5):67–76

Blanksvärd T, Täljsten B, Carolin A (2009) Shear strengthening of concrete structures with the use of mineral-based composites. J Compos Constr 13(1):25–34

Brückner A, Ortlepp R, Curbach M (2006) Textile reinforced concrete for strengthening in bending and shear. Mater Struct 39:741–748

Carolin A, Täljsten B (2005) Theoretical study of strengthening for increased shear bearing capacity. J Compos Constr 9(6):497–506

D'Ambrisi A, Focacci F (2011) Flexural strengthening of RC beams with cement based composites. J Compos Constr 15(5):707–720

Fib bulletin 14 (2001) Externally bonded FRP reinforcement for RC structures. Technical report, International Federation for Structural Concrete, Lausanne, Switzerland

Loreto G, Leardini L, Arboleda D, Nanni A (2013) Performance of RC slab-type elements strengthened with fabric-reinforced-cementitious-matrix (FRCM) composites. J Compos Constr 18(3):1090–0268

Nanni A (2012) FRCM strengthening—a new tool in the concrete and masonry repair toolbox. Concr Intern Des Constr 34(4):43–49

Ombres L (2011) Flexural analysis of reinforced concrete beams strengthened with a cement based high strength composite material. Compos Struct 94(1):143–155

Ombres L (2012) Debonding analysis of reinforced concrete beams strengthened with fiber reinforced cementitious mortar. Eng Fract Mech 81:94–109

Papanicolaou CG, Triantafillou TC, Papathanasiou M, Karlos K (2008) Textile reinforced mortar (TRM) versus FRP as strengthening material of URM walls: out-of-plane cyclic loading. Mater Struct 41(1):143–157

Parisi F, Iovinella I, Balsamo A, Augenti N, Prota A (2013) In-plane behaviour of tuff masonry strengthened with inorganic matrix–grid composites. Compos B 45(1):1657–1666

Peled A, Mobasher B (2007) Tensile behavior of fabric cement-based composites: pultruded and cast. J Mater Civ Eng 19(4):340–348

Popov EP (1999) Engineering mechanics of solids. Prentice-Hall, Upper Saddle River

Triantafillou TC, Papanicolaou CG (2006) Shear strengthening of reinforced concrete members with textile reinforced mortar (TRM). Mater Struct 39(1):93–103